4-Hydroxyequilenin-Adenine Lesions in DNA Duplexes: Stereochemistry, Damage Site, and Structure†

Shuang Ding,‡ Robert Shapiro,‡ Nicholas E. Geacintov,‡ and Suse Broyde*,§

Department of Chemistry and Department of Biology, New York University, 100 Washington Square East, New York, New York 10003

Received August 14, 2006; Revised Manuscript Received October 17, 2006

ABSTRACT: The equine estrogens, equilin and equilenin, are major components of the drug Premarin, the most widely used formula for hormone replacement therapy. The derivative 4-hydroxyequilenin (4-OHEN), a major phase I metabolite of equilin and equilenin, autoxidizes to potent cytotoxic quinoids that can react in vitro and in vivo with cytosine and adenine in DNA. Unique cyclic adducts containing the same bicyclo[3.3.1]nonane-type connection ring are produced. Each base adduct has four stereoisomers. In order to elucidate the structural effects of A versus C modification, we have carried out molecular dynamics simulations of the stereoisomeric 4-OHEN-A adducts in DNA 11-mer duplexes and compared results with an earlier study of the C adducts (Ding, S., Shapiro, R., Geacintov, N.E., and Broyde, S. (2005) Equilenin-Derived DNA Adducts to Cytosine in DNA Duplexes: Structures and Thermodynamics, *Biochemistry 44,* 14565−14576). Similar stereochemical principles govern the orientations in DNA duplexes of the 4-OHEN-A adducts as for the analogous C adducts, with opposite orientations of the equilenin rings in stereoisomeric pairs of adducts characterized by near-mirror image circular dichroism (CD) spectra. However, the larger purine adducts have unique structural properties in the duplexes that distinguish their characteristics from those of the pyrimidine adducts. Significant differences are observed in terms of hydrogen bonding, stacking, bending, groove dimensions, solvent exposure, and hydrophobic interactions; also, each of the four stereoisomeric 4-OHEN-A adducts exhibit distinct structural features. Each base adduct and stereoisomer distorts the structure of the DNA duplex differently. These characteristics may manifest themselves in terms of differential nucleotide excision repair susceptibilities and mutagenic activities of the 4-OHEN-A and C adducts.

Continuous exposure to estrogens through hormone replacement therapy (HRT) has been shown to increase the risk of breast cancer (*1*−*7*). The HRT drug Premarin contains equine estrogens, namely equilin and equilenin. 4-Hydroxyequilenin (4-OHEN), a phase I metabolite of both equilin and equilenin, autoxidizes to potent cytotoxic quinoids (*8*, *9*) that can cause a variety of DNA lesions in vitro and in vivo (*10*−*15*), including the formation of stable adducts produced by alkylation (*12*, *16*). Such adducts, if not repaired efficiently, may cause mutations that, in turn, may initiate carcinogenesis (*17*).

The quinoids produced by 4-OHEN oxidation can react with the nucleosides dG, dA, and dC to form unusual stable cyclic bulky adducts (*9*, *16*, *18*), and four stereoisomeric adducts have been identified with each of these three bases (*19*). The chemical structures of these adducts have been determined by electrospray MS and NMR methods (Figure 1) (*16*, *18*, *19*). 4-OHEN-dG and dA adducts have been found in vivo when 4-OHEN is injected into the mammary fat pads of rats (*12*). The dG, dA, and dC adducts have also been detected in human breast cancer patients who use Premarin (*20*). The formation of 4-OHEN adducts has been investigated in detail with the single-stranded oligonucleotides 5′-d(CCATCGCTACC) and its complementary strand in vitro (*21*). The yield of these adducts is influenced by the sequence and secondary structures of DNA. Reaction with cytosine is overwhelmingly preferred over adenine. Guanine adducts are observed in olignucleotides that contain only G and unreactive T residues.

The conformations of the stereoisomeric 4-OHEN adducts on the base level have been previously determined by density functional theory (DFT) quantum mechanical methods (*22*). For 4-OHEN-C and A adducts (Figure 1), the essential structural feature is the near-perpendicular orientation of the equilenin and bridge-linked base, whose Watson−Crick edge is obstructed. The chirality of the C3′ atom determines the handedness of the equilenin rings, and the absolute configuration of the C2′ atom governs the orientation of its OH group. The unsaturated bicyclo[3.3.1]nonane-type linkage site causes the conformations of the 4-OHEN-A and C adducts to be severely restricted. Only one conformer was obtained for each adduct. Near mirror image conformations in the stereoisomer adduct pairs C1/C2 (A1/A2) and C3/C4 (A3/A4) were found. This is consistent with near-mirror image

† This research is supported by an NIH grant (CA-75449) to S.B., an NIH grant (CA-73638) subcontracted from the University of Illinois at Chicago (J. Bolton, P.I.), and an NIH grant (CA-112412) to N.E.G.

* Corresponding author. Telephone: (212) 998-8231. Fax: (212) 995-4015. E-mail: broyde@nyu.edu.

‡ Department of Chemistry.

§ Department of Biology.

10.1021/bi061652o CCC: $37.00
Published on Web 12/10/2006

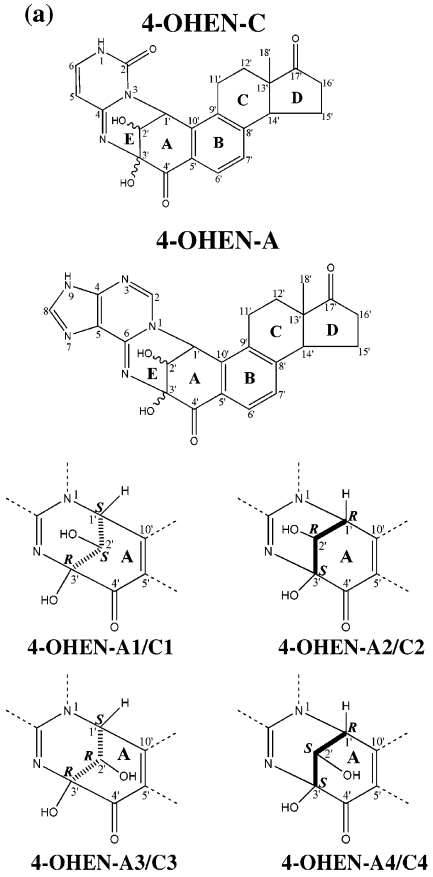

FIGURE 1: (a) Chemical structures and stereochemical characteristics of the 4-OHEN-A and C adducts. (b) Sequence of the 11-mer B-DNA duplex for the MD simulations. A_4* is the damaged position.

circular dichroism (CD) spectra of each stereoisomeric pair observed experimentally (*21*).

In previous work, the structures and thermodynamics of 4-OHEN-C adducts were investigated in 11-mer duplexes by computational and modeling methods (*23*). Our results showed that the covalently linked cytosine residue can adopt the *syn* or *anti* glycosidic bond conformations, placing the equilenin in the B-DNA major or minor groove, respectively. In each structural family, opposite orientations of the equilenin ring system, the C18′ bulky methyl group, and the bridge ring C2′ OH group were found in the stereoisomer pairs. Moreover, the stereoisomeric lesions distort the DNA duplexes differentially.

Here, we present molecular modeling and molecular dynamics (MD) simulation studies of the 4-OHEN-A adducts in DNA 11-mer duplexes. Stereochemical characteristic and duplex structural properties were compared with the analogous 4-OHEN-C adducts. The stereochemical effects in the 4-OHEN-C and A adducts are similar. However, we find structural differences in the duplexes containing stereochemically similar cytosine and adenine adducts in bending, groove dimensions, hydrogen bonding, stacking interactions, solvent exposure, and hydrophobic interactions, which reflect the nature of the base modified. These differences may underlie differential mutagenicities and repair susceptibilities of the stereoisomeric modified adenine and cytosine bases (*24*−*30*).

METHODS

Starting Structures. A model of the unmodified sequence was created in a standard B-DNA conformation and energy-minimized with DUPLEX (*31*). The conformations of the 4-OHEN-A base adducts were obtained from the previous DFT optimizations (*22*). The A_4 residue of the selected 11-mer DNA sequence was replaced with each of the four 4-OHEN-A adducts. Then, the modified base was rotated through the glycosidic torsion angle χ to locate domains with minimal steric close contacts. In each case, a narrow region was found in the *syn* domain. The equilenin moiety is located in the major groove (Figure S1). In the *anti* conformational domain, however, no structures without collisions were obtained in the initial models. The fewest close contacts occurred when the equilenin was inserted between the Watson−Crick hydrogen-bonding edge of an adjacent base pair. Table S1 (Supporting Information) gives χ values of the adducts employed in all 4-OHEN-A starting models.

Force Field. The AMBER 8 program package (*32*), the Cornell et al. force field (*33*), and the parm99.dat parameter set (*34*) were employed to perform MD simulations. Force field parameters for 4-OHEN-A adducts that were not in the AMBER force field were developed, consistent with the rest of the AMBER force field. Bond length, bond angle, and dihedral angle equilibrium values were taken from the DFT optimized conformations. The force constants for bonds and angles were obtained by analogy with chemically similar atom types in the AMBER force field. The force constants for bond angles containing the N atom at the linkage site of the 4-OHEN-A adduct (Figure 1) were obtained from those of the analogous 4-OHEN-C adducts (*23*). Table S2 gives all the added force field parameters for the 4-OHEN-A stereoisomers. The partial charges of the modified nucleotide were calculated with two stages of RESP (*35*−*37*) in the AMBER package. Geometry optimization with HF/6-31G* was first carried out for the modified nucleoside with initial models whose glycosidic torsion χ was *syn* (Table S1) using Gaussian 98 (*38*). Then, the least-squares charge-fitting algorithm RESP (*35*, *37*) in the AMBER package was used to fit the derived electrostatic potentials from Gaussian to the atomic center of each molecule. Atom types, topology assignments, and partial charges are listed in Table S3.

Molecular Dynamics Protocol. MD simulations were carried out for the unmodified control and all eight 4-OHEN-A initial models (an *anti* and a *syn* model for each stereoisomer, Figure S1 and Table S1). Details of the MD protocol (*32*, *39*−*44*) are given in the Supporting Information.

Stability of the Molecular Dynamics Simulation. MD simulations of the 4-OHEN-A adducts and the unmodified control were carried out for 5 ns. The structures generally fluctuate stably after 1 ns, and the last 4 ns time frame was employed for our further analyses. In the case of *anti* 4-OHEN-A4, the simulation was extended to 9 ns to obtain reasonable stability; the last 4 ns were employed for analyses. Plots of root mean square deviations (rmsd) of the current structure relative to the average structure, as a function of time, are shown in Figure S2.

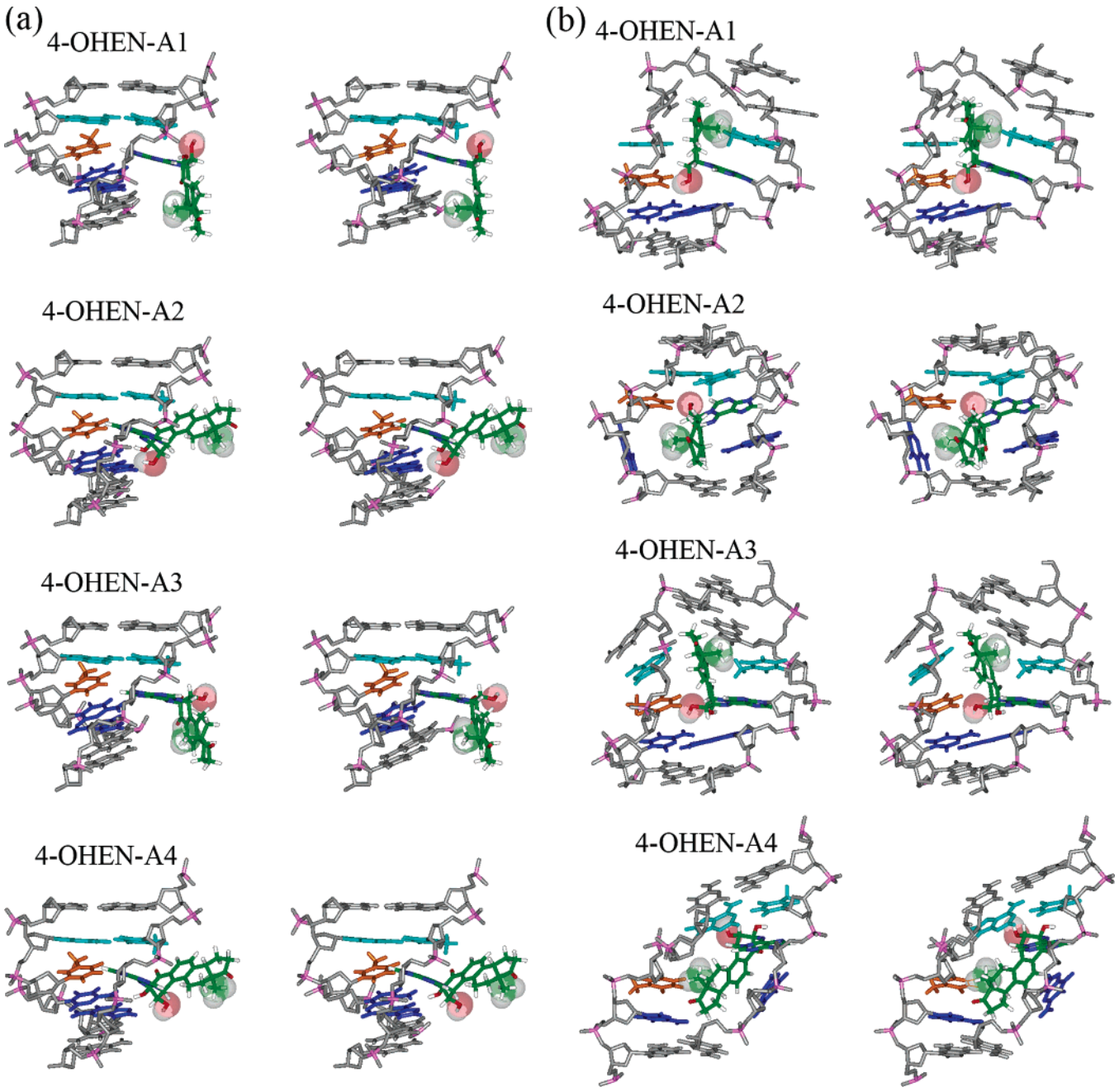

FIGURE 2: Five base pair segments with modified bases at center in the trajectory-average structures for the four 4-OHEN-A modified duplexes in stereoview. The color code is as follows. 4-OHEN-A, colored by atom: C, green; O, red; N, blue; H, white; partner base T, orange; 5′-side T_3·A_{20} pair, light blue; 3′-side G_5·C_{18} pair, dark blue. The C2′ OH group of the adduct is in pink spheres, and the C18′ methyl group is in green spheres. (a) *Syn* glycosidic conformation. (b) *Anti* glycosidic conformation. In 4-OHEN-A1 and A3, 6-mers at 5′-end of the modified strand are shown.

Structural Analyses. The PTRAJ and CARNAL modules of AMBER were employed for structural analyses. Stacking interactions were estimated by computing the van der Waals interaction energies between adjacent base pairs, including the damaged adenine and partner T pair with the program ANAL of AMBER. The equilenin moiety, nearly perpendicular to the attached adenine residue, is not included in the base stacking interactions. In addition, DNA duplex groove dimensions for the ensemble of structures for each stereoisomer were computed with MD Toolchest (*45*, *46*). We computed the bend angle of the duplex with the CURVES program (*45*), employing the "UU" option. The first and last base pairs were removed prior to this analysis. In addition, we removed the modified base because CURVES could not recognize this moiety. Thus, the computed bend angles were based on global helix axes determined by the central 9-mer but excluding the modified adenine. The solvent accessible surface area for the equilenin moiety was computed using the Connolly algorithm (*47*) implemented in the InsightII program with a probe radius of 1.4 Å.

Free Energy Analyses. The molecular mechanics Poisson−Boltzmann surface area (MM−PBSA) method (*48*−*54*) in AMBER was employed for thermodynamic analyses. Details of the free energy calculations (*48*, *49*, *55*−*60*) are given in the Supporting Information.

InsightII from Accelrys, Inc. was employed for visualization and model building. Computations were carried out on our own cluster of Silicon Graphic Origin supercomputers

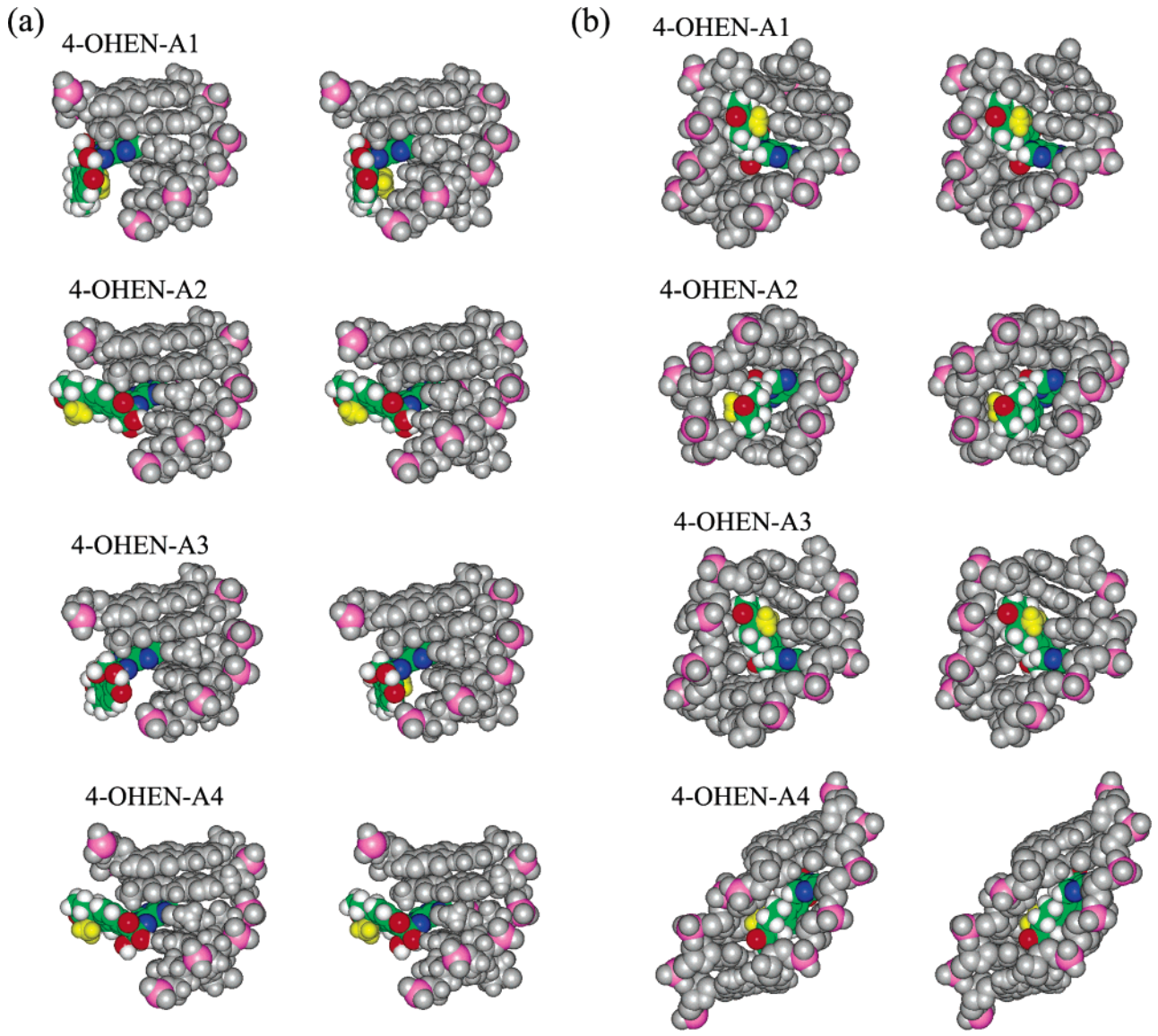

FIGURE 3: Space filling models of five base pair segments with modified bases at center in the trajectory-average structures for the four 4-OHEN-A modified duplexes in stereoview. The color code is as follows. 4-OHEN-A, colored by atom: C, green; O, red; N, blue; H, white (except the methyl group in yellow). (a) *Syn* glycosidic conformation. (b) *Anti* glycosidic conformation. In 4-OHEN-A1 and A3, 6-mers at 5′-end of the modified strand are shown.

and Octane workstations, as well as at the New York University Information Technology Services supercomputers.

RESULTS AND DISCUSSION

Starting Models

We employed the sequence of Figure 1, which is also under experimental investigation (*21*). This duplex is the same as the one employed in our study of the 4-OHEN-C adducts, where modification was at C_{18} of the complementary strand. Each stereoisomeric 4-OHEN-A adduct was modeled into the 11-mer B-DNA duplex, with the lesion glycosidic bond in both *syn* and *anti* domains, as described in Methods. In the *syn* conformation, the adducts reside in the major groove; in the *anti* conformation, they are inserted into the duplex with extensive collisions in the initial structures. Molecular dynamic simulations were carried out for all starting models (Figure S1).

Structural Analyses

Stereochemical Characteristics: Opposite Orientations in Stereoisomer Pairs. Stereochemistry plays an important role in determining the specific structural properties of the 4-OHEN adducts. The stereochemistry of the 4-OHEN-C and A adducts are dependent on the absolute configurations of substituents at C2′ and C3′ of the linkage site (Figure 1). The stereochemical characteristics of the 4-OHEN-C adducts are therefore retained in the 4-OHEN-A adducts. Structures of the four stereoisomeric 4-OHEN-A adducts in *syn* and *anti* glycosidic conformations are shown in Figures 2 and 3. With the glycosidic bond *syn*, the equilenin rings are situated in the major groove, 5′ directed in 4-OHEN-A2 and A4, and 3′ directed in 4-OHEN-A1 and A3. The collisions in the initial *anti* models were relieved during the dynamics by repositioning the equilenin rings to protrude into the minor groove. In these structures with the glycosidic torsion angles in the *anti* conformation, the equilenin rings are directed to

Table 1: Stereochemistry-Dependent Structural Properties of 4-OHEN-A/C Adducts

		syn conformation			*anti* conformation		
stereochemistry		equilenin rings orientation[a]	C18' methyl group[b,c]	C2' OH group	equilenin rings orientation[a]	C18' methyl group[c,d]	C2' OH group
4-OHEN-A1/C1	2'S−3'R	3'	M	near axial	5'	M	near axial
4-OHEN-A2/C2	2'R−3'S	5'	S	near axial	3'	P	near axial
4-OHEN-A3/C3	2'R−3'R	3'	M	near equatorial	5'	M	near equatorial
4-OHEN-A4/C4	2'S−3'S	5'	S	near equatorial	3'	P	near equatorial

[a] With respect to the modified strand. [b] S: toward solvent. [c] M: toward modified strand. [d] P: toward partner strand.

Table 2: Hydrogen Bonds and Occupancies Involving the A_4* or Partner T_{19}[a]

syn	hydrogen bond	occupancy (%)
4-OHEN-A1	(T_{19})O4...H−N6(A_{20})	22.9
4-OHEN-A2	(A_4*)O3'−H...O6(G_5)	53.9
	(A_4*)O2'−H...N7(G_5)	44.0
	(A_4*)O2'−H...O6(G_5)	29.5
	(A_4*)O2'−H...N7(G_{17})	19.5
	(A_4*)O3'...H−N4(C_{18})	24.3
	(A_4*)N6...H−N4(C_{18})	22.0
	(A_4*)N7...H−N3(T_{19})	69.7
	(T_{19})O4...H−N6(A_{20})	34.9
4-OHEN-A3	(A_4*)O4'...H−N4(C_{16})	52.4
	(T_{19})O4...H−N6(A_{20})	39.6
4-OHEN-A4	(A_4*)O3'−H...O6(G_5)	85.0
	(A_4*)N7...H−N3(T_{19})	60.3
	(T_{19})O4...H−N6(A_{20})	30.5
anti	hydrogen bond	occupancy (%)
4-OHEN-A1	(A_4*)O2'−H...O2(T_{19})	93.4
	(A_4*)O3'...H−N3(T_{19})	51.2
4-OHEN-A2	(A_4*)O2'−H...O4(T_3)	39.2
	(A_4*)O2'−H...O3'(A_4*)	24.1
	(A_4*)O4'...H−N2(G_5)	54.1
	(A_4*)O2'...H−N3(T_{19})	84.8
	(T_{19})O4...H−N6(A_{20})	28.3
4-OHEN-A3	(A_4*)O2'...H−N3(T_{19})	50.9

[a] Hydrogen bonding criteria were 3.35 Å between heavy atoms with a hydrogen bonding angle for donor−hydrogen−acceptor of 135°.

the 5′-side of the modified strand in 4-OHEN-A1 and A3 and to the 3′-side in 4-OHEN-A2 and A4. The stereochemical properties of the 4-OHEN-C and A isomers also govern the orientations of the methyl group and the C2′ OH group in DNA duplexes. The stereochemical characteristics of the four stereoisomeric 4-OHEN-A and C adducts are given in Table 1.

Hydrogen Bonding Interactions. (i) Syn Glycosidic Conformation. Watson−Crick hydrogen bonds are retained in all the base pairs, except for the modified base and its partner (Figure 2). However, in the *syn* conformation, the N7 of the modified adenine may hydrogen bond with N3H of its partner T_{19}. This is observed with an occupancy of ∼60% of the trajectory in the 4-OHEN-A2 and A4 stereoisomeric adduct simulations (Table 2). However, crowding between the bridge ring of the adduct and the methyl group of T_3 inhibits formation of this hydrogen bond in 4-OHEN-A1 and A3. In all cases, T_{19} has sufficient flexibility to hydrogen bond with N6H of the 5′-side A_{20}. In addition, each stereoisomer has unique hydrogen bonding interactions with base atoms on the damaged or partner strand, except for 4-OHEN-A1. Table 2 summarizes these interactions.

(*ii) Anti Glycosidic Conformation.* In the *anti* conformation, the equilenin rings were repositioned during the dynamics to protrude into the minor groove, thus severely disrupting Watson−Crick hydrogen bonding interactions of adjacent, unmodified base pairs (Figure 2). Watson−Crick hydrogen bonding of the G_5•C_{18} pair is totally disrupted in the 3′-directed 4-OHEN-A2 and A4 isomeric adducts. For the 5′ oriented 4-OHEN-A1 and A3 cases, all the 5′-side Watson−Crick unmodified base pairs are broken (see below). In the *anti* case, the hydroxyl groups of the adduct linkage site point to the hydrogen bond edge and can form hydrogen bonds with the partner base T_{19}, except in the case of A4, which does not participate in any hydrogen bond interactions due to unusual stacking (see below). In addition, 4-OHEN-A2 and its partner T_{19} form hydrogen bonds with adjacent bases (Table 2).

Stacking. (i) Syn Glycosidic Conformation. The modified adenine is mainly stacked within the DNA duplex (Figures 2a and 3a). However, base pair stacking is significantly perturbed, in line with the absence of Watson−Crick hydrogen bonding at the lesion sites. The 4-OHEN-A2 and A4 adducts exhibit better stacking interactions, because the modified adenine forms a hydrogen bond with its partner, which diminishes the base pair stacking perturbation (Table S4).

(*ii) Anti Glycosidic Conformation.* The modified adenine bases assume mainly stacked conformations within the DNA duplexes (Figures 2b and 3b). However, in 4-OHEN-A2 and A4, the stacking is diminished due to disrupted Watson−Crick hydrogen bonding of the adjacent unmodified base pair G_5•C_{18}. The presence of the large A2 and A4 adducts also tilts the adjacent bases C_{18} and G_5, respectively. This severely weakens the stacking interactions involving the pair G_5•C_{18}. However, in 4-OHEN-A4, the tilted base G_5 stacks with the equilenin aromatic B ring, and the partner T_{19} now stacks only with C_{18}. In 4-OHEN-A1 and A3, C_{21} is pushed away from its normal base pair position by the equilenin rings and stacks with A_{20} but not C_{22}. Consequently, the 3′-end base C_{22} slips into the C_{21} position, and in 4-OHEN-A3, Watson−Crick hydrogen bonds are formed between C_{22} and G_2 but not in the case of A1 (Figure 2). This causes the 5′-end G_1, a dangling end without a partner, to stack with the misaligned C_{22}•G_2 pair. Likely, this unusual stacking is an end effect due to the position of the 5′-directed adduct only three base pairs away from the C_{22}•G_1 terminus.

Bending and Groove Dimensions. (i) Syn Glycosidic Conformation. The modified duplexes are somewhat bent as compared to the unmodified duplex (Table 3), with 4-OHEN-A1 and A3 more bent than 4-OHEN-A2 and A4.

Table 3: Trajectory Average Bend Angles of the Modified DNA Duplexes[a]

	unmodified	4-OHEN-A1	4-OHEN-A2	4-OHEN-A3	4-OHEN-A4
syn	15.2 (7.7)	29.5 (15.4)	23.9 (11.4)	30.8 (13.4)	22.9 (9.1)
anti		41.5 (10.9)	54.1 (20.0)	48.1 (20.2)	55.0 (21.8)

[a] Bend angles are in degrees. Standard deviations are in parentheses.

It appears that the hydrogen bond between the modified adenine N7 and its partner T_{19} limits the bending in A2 and A4. The major groove width around the lesion site is generally enlarged due to accommodation of the equilenin rings (Figure 4), although only modestly in the case of 4-OHEN-A3 because of a hydrogen bond between the carbonyl group of the equilenin with N4H of C_{16}. The dimensions of the minor groove in the *syn* 4-OHEN-A adducts fluctuate around those of the unmodified duplex.

(*ii*) *Anti Glycosidic Conformation.* In the *anti* conformation, the 4-OHEN-A modified duplexes are significantly more bent than in the *syn* conformers (Table 3). The broken base pairs adjacent to the lesion in each stereoisomeric adduct provide added flexibility, which allows a greater bend. The minor groove opens because the adducts protrude into it, except in the case of 4-OHEN-A4, in which stacking between the equilenin B ring and G_5 causes major groove enlargement. The minor groove opening is in the direction of the equilenin ring orientation in each case.

Table 4: Solvent Accessible Surface for the Equilenin Rings of 4OHEN-C and A Adducts in 11-Mer Duplexes

	4-OHEN-A1	4-OHEN-A2	4-OHEN-A3	4-OHEN-A4
syn	250.3 (7.1)	220.9 (15.7)	243.3 (10.9)	229.7 (9.6)
anti	123.0 (10.1)	163.1 (13.7)	131.4 (26.7)	201.1 (20.1)
	4-OHEN-C1	4-OHEN-C2	4-OHEN-C3	4-OHEN-C4
syn	232.0 (9.7)	193.6 (8.2)	222.0 (6.4)	212.4 (7.4)
anti	151.9 (11.1)	112.9 (6.5)	131.3 (6.6)	115.3 (6.6)

[a] Trajectory average values for solvent accessible surface (Å^2) of equilenin moiety. Standard deviations are given in parentheses. 4-OHEN-C adduct values are based on trajectories of ref 23.

Solvent Exposure. The different groove positions of the *syn* and *anti* conformations cause a large difference in solvent exposure of the adducts. In the *syn* case, the equilenin moiety is positioned in the major groove without much distortion of the duplex structures, but it is mostly exposed to the solvent (Figures 2a and 3a). In contrast, the equilenin moiety in the *anti* adducts is much less solvent exposed. The bulky rings protrude to the smaller minor groove and have hydrophobic interactions with the DNA backbone (Figures 2b and 3b). The solvent accessible surface of the equilenin moiety (Table 4) clearly shows this difference between the *syn*/major groove and *anti*/minor groove conformations.

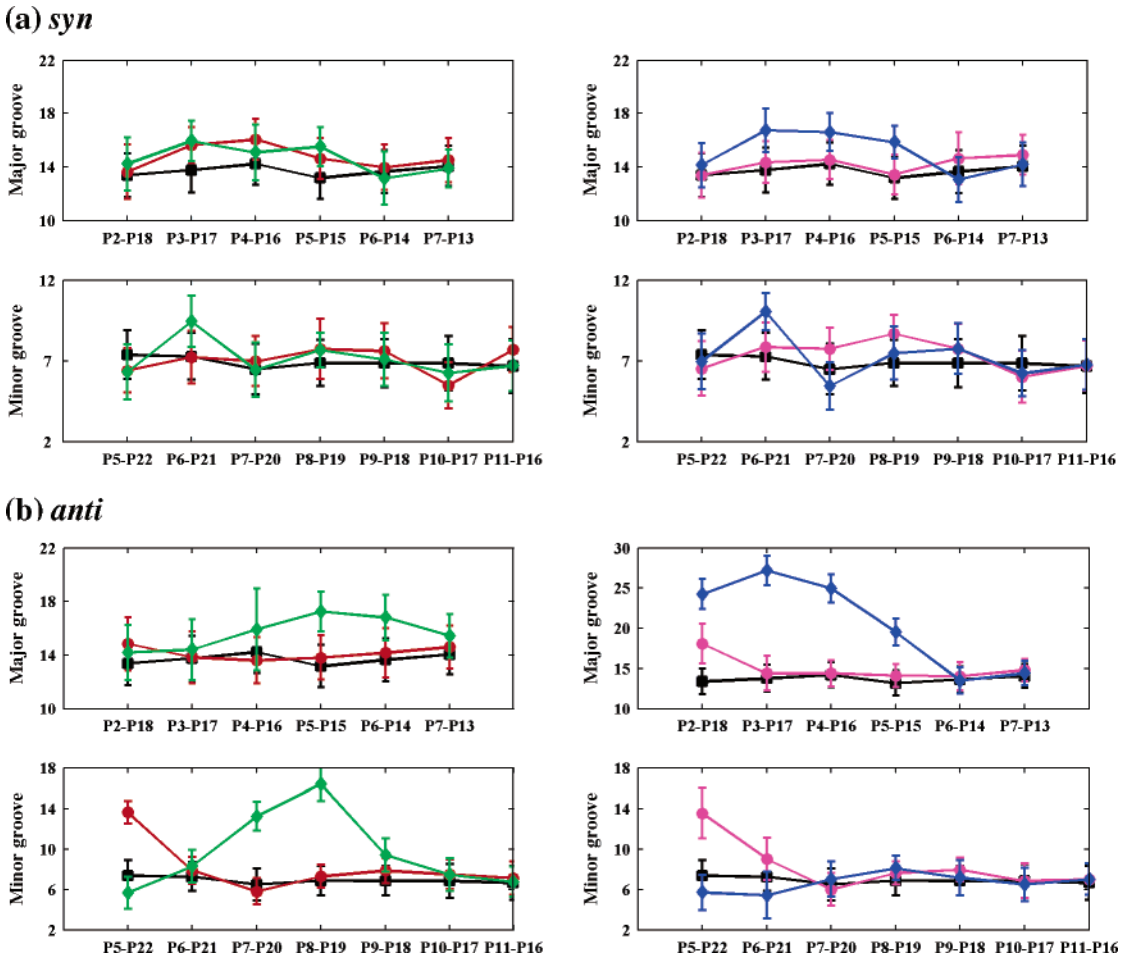

FIGURE 4: Trajectory-average groove dimensions with standard deviations (Å) of 4-OHEN-A modified duplexes. The color code is as follows: 4-OHEN-A1, red; 4-OHEN-A2, green; 4-OHEN-A3, magenta; 4-OHEN-A4, blue; unmodified duplex, black. (a) *Syn* glycosidic conformation. (b) *Anti* glycosidic conformation.

Table 5: Relative Free Energies for *Syn* and *Anti* Conformations of Each Stereoisomeric Adduct[a]

	4-OHEN-A1	4-OHEN-A2	4-OHEN-A3	4-OHEN-A4
syn	3.6	0	5.4	0.6
anti	0	6.3	0	0
	4-OHEN-C1	4-OHEN-*C*2	4-OHEN-C3	4-OHEN-C4
syn	0	3.9	0	5.0
anti	1.5	0	6.8	0

[a] For each stereoisomeric adduct, the conformation with the lower energy is assigned $\Delta G = 0$. Energies are in kcal/mol. Data for 4-OHEN-C adducts are from ref 23.

Thermodynamic Analyses

The ensemble of structures from the simulations were employed to carry out thermodynamic analyses using the MM−PBSA method (*48*−*54*). Relative free energies of *syn* and *anti* conformations were calculated to compare their conformational stabilities (Table 5 and S5). We note that the *anti*/minor groove conformation, being lowest in energy for A1, A3, and A4, is mainly favored. The solvent exposed surface plays an important role in the conformational stability of these adducts in DNA duplexes. In the *anti*/minor groove case, the equilenin rings have less solvent accessible surface with attendant better hydrophobic interactions (Figure 3). This favors the *anti* conformation. However, the *syn*/major groove conformation is less distorted, as described above. The conformational preference is a balance between these structural features in each stereoisomer. The diminished solvent exposure with enhanced hydrophobic contacts causes the *anti* conformation to be preferred, except for 4-OHEN-A2. In this case, the purine ring system causes unfavorable unstacking of C_{18} with exposure to solvent of this base and the equilenin (Figures 2 and 3). A similar unstacking involving G_5 occurred also in 4-OHEN-A4 but was compensated for by stacking of this base with the equilenin. Thus, our results indicate that both *syn* and *anti* conformers with the adduct in the major or minor groove, respectively, are feasible. A subtle interplay of the adduct groove position and attendant solvent exposure/hydrophobic contacts and adduct-induced distortion determine the conformational preference of each stereoisomeric adduct; environmental conditions, such as salt concentration, base sequence context, and duplex length, could influence the choice.

Comparison of 4-OHEN-A and C Adducts

The 4-OHEN-A adducts have the same bicyclo[3.3.1]-nonane-type connection rings as 4-OHEN-C. Consequently, similar stereochemical characteristics as in the 4-OHEN-C stereoisomers, described previously (*23*), were obtained for the analogous 4-OHEN-A adducts (Table 1). For each groove position, the equilenin ring orientations are the same for 4-OHEN-C and A adducts with the same stereochemistry; thus, the opposite orientation effect in stereoisomer pairs is the same. Preliminary NMR data for 4-OHEN-dC adducts have suggested opposite orientations of stereoisomers in duplex DNA (Zhang, N., Kolbanovskiy, A., Ding, S., Shastry, A., Geacintov, N. E., Broyde, S., and Patel, D., personal communication). However, there are subtle differences that are governed by the nature of the base damaged. The solvent accessible surface of the equilenin moiety plays a role here. Hence, we calculated this quantity for the cytosine adducts to compare with adenine (Table 4). We also present in Table 5 the *syn*/*anti* preference of the cytosine adducts for comparison. We note that this preference for the C and A adducts is inverted in every case, except for A4, whose *syn* and *anti* structures are almost equal in energy. Thus, C1 and C3 prefer *syn* and C2 and C4 prefer the *anti* conformation. As described above, the *syn*/major groove conformers are mainly favored by less distortion; the *anti*/minor groove structures are favored by diminished solvent exposure with attendant enhanced favorable hydrophobic contacts. Each stereoisomer and base adduct selects a different balance between these competing features. For the 4-OHEN-C case, in C2 and C4, the favorable hydrophobic contacts in *anti* dominate; in C1 and C3, the lack of distortion with favorable van der Waals interactions between the inward-facing equilenin methyl group and adjacent base in *syn* dominate (Figure 5). In A1 and A3, these methyl groups in *syn* are too far from the DNA for such contacts, because of the larger purine ring system. The purine in *anti* A2 causes unfavorable unstacking and solvent exposure, as described above (Figures 2 and 3).

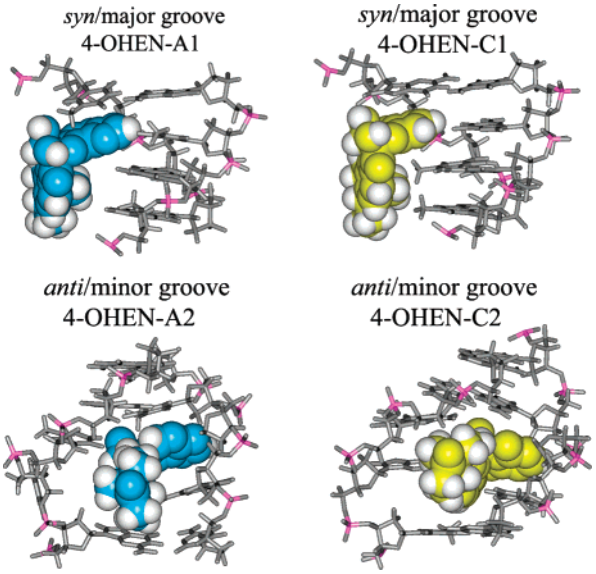

FIGURE 5: Comparison of *syn*/major groove and *anti*/minor groove structures of 4-OHEN adducts to adenine and cytosine. Five base pair segments with modified bases at center are shown. Note that equilenin rings are usually more solvent-exposed in A than in C adducts (Table 4). The color code is as follows: 4-OHEN-A in blue with hydrogen in white; 4-OHEN-C in yellow with hydrogen in white.

Table 6 gives a structural comparison of 4-OHEN-C and A adduct duplex distortions. We note from the table that each base adduct and each stereoisomer produces distinct structural distortions in terms of hydrogen bonding, stacking, bending, and groove dimensions. Each perturbs the structure of the DNA duplex differently. Overall, compared to the C adducts, the equilenin rings of the A adducts in the *syn* conformation are positioned further away from the DNA in the major groove due to the larger purine ring, which results in more solvent exposed equilenin rings and less distorted major grooves. Furthermore, in *syn*, the larger 4-OHEN-A adducts generally disturb the stacking more and the DNA duplexes bend more toward the major groove in an effort to shield these adducts from the solvent. In the *anti* case, both

Table 6: Comparison of 4-OHEN-C[a] and A Adduct Features Compared to Unmodified Control

syn	adjacent base pair[b]	number of adduct hydrogen bonds[c]	stacking energy difference[d] (kcal/mol)	bend angle difference[e] (deg)	major groove distortion[f] (Å)	minor groove distortion[f] (Å)
4-OHEN-C1	intact	0	5.5	11.9	3.1	0.7
4-OHEN-A1	intact	0	5.9	14.3	1.8	−1.3
4-OHEN-C2	intact	1	4.6	11.0	3.1	2.0
4-OHEN-A2	intact	2	4.7	8.7	2.3	2.1
4-OHEN-C3	intact	0	5.3	−0.7	−2.2	−2.3
4-OHEN-A3	intact	1	6.6	15.6	1.0	1.8
4-OHEN-C4	distorted	2	9.2	0.1	5.3	−6.0
4-OHEN-A4	intact	2	3.1	7.5	2.9	2.7
anti	adjacent base pair[b]	number of adduct hydrogen bonds[c]	stacking energy difference[d] (kcal/mol)	bend angle difference[e] (deg)	major groove distortion[f] (Å)	minor groove distortion[f] (Å)
4-OHEN-C1	distorted	0	22.2	4.1	5.2	8.8
4-OHEN-A1	broken	2	*g*	26.3	1.4	6.2
4-OHEN-C2	broken	1	19.7	15.8	3.7	−2.6
4-OHEN-A2	broken	2	22.1	38.9	4.1	9.5
4-OHEN-C3	broken	3	22.6	38.4	2.2	8.2
4-OHEN-A3	broken	1	*g*	32.9	4.7	6.1
4-OHEN-C4	broken	2	15.9	40.1	2.8	1.6
4-OHEN-A4	broken	0	20.9	39.8	13.4	−1.9

[a] Data for 4-OHEN-C from ref 23. [b] Occupancy of Watson−Crick hydrogen bonds: intact, all >90%; distorted, any one 50%-90%; broken, all 0%. Hydrogen bonds are distorted or broken in the direction of the equilenin ring orientation (Figure 2), except for *anti* C1. The unmodified duplex has all base pairs intact. [c] Number of hydrogen bonds involving 4-OHEN base adduct with occupancy >50% in stable time frame of trajectory (see Methods and Table 2). [d] Difference between stacking interaction energy of modified duplex and its unmodified counterpart (see Methods and Table S4). Larger energies show more perturbed stacking. [e] Difference between the trajectory average bend angle of the adduct and the unmodified duplex (Table 3). [f] Using the unmodified duplex as reference, we calculated the groove distortions of the modified duplexes as $(d - d_0)$, where d is a groove dimension of the modified duplex and d_0 is the corresponding value for the unmodified duplex (Figure 3). The groove dimension difference with the largest absolute value is shown. A negative sign indicates groove closing compared to the unmodified control. [g] Stacking cannot be calculated due to the dangling end.

4-OHEN-C and A adducts generally break adjacent Watson−Crick base pairs. However, the larger 4-OHEN-A adducts also tilt nearby bases in order to accommodate the equilenin rings in the minor groove (Figure 2). This causes the weaker stacking and larger groove distortions in the A adducts. However, stereoisomer effects involving adduct hydrogen bonds with neighboring bases can modulate these overall tendencies in specific cases.

Structure−Function Relationships

Our modeling studies indicate structural properties that are distinct for each stereoisomer and base damaged. These structural differences likely account for observed differences in biochemical function. In vitro primer extension studies conducted with several Y-family bypass polymerases indicate that various 4-OHEN-C and A lesions are differentially bypassed, depending on stereochemistry and base damaged (*24*, *26*−*28*). Adduct stereochemistry effects on bypass efficiency were observed with pol η. Specifically, the bypass frequency in pol η differed by 2 orders of magnitude in the members of a pair of 4-OHEN-dC stereoisomers with opposite sign CD spectra (*27*). For 4-OHEN-dA adducts, the bypass frequency past one stereoisomer was approximately 3 times higher than that for another (*28*). For a pair of 4-OHEN-dC major adducts whose CD spectra were of opposite sign, with pol κ mismatched dCMP and dAMP were inserted opposite both stereoisomers, and chain extension with partner dC was much higher than that with dA (*27*). Insertion of dGMP, the correct base, was highly inefficient. For this 4-OHEN-dC pair with pol η, insertion of dAMP and extension were both higher than that for the correct base dGMP. However, for the pair of 4-OHEN-dA major adducts with opposite sign CD spectra, both pols κ and η preferentially incorporated dTMP, the correct base, opposite these 4-OHEN-dA lesions; mismatched dAMP and dCMP were also incorporated by pol κ and η, respectively (*28*). Current studies also suggest damaged base-specific repair susceptibilities, with dA adducts less repaired than dC adducts in prokaryotic and eukaryotic nucleotide excision repair (NER) assays (*26*, *30*) (Kropachev, K., Chen, D., Kolbanovskiy, M. and Geacintov, N., to be published).

CONCLUSION

The 4-OHEN-A adducts have the same connection rings as the 4-OHEN-C adducts; this produces similar stereochemical properties and stereochemistry-governed orientations in DNA duplexes. However, the larger purine adducts cause distinctly different structural properties as compared to the smaller pyrimidine adducts. Specific features of hydrogen bonding, bending, stacking, groove dimensions, solvent exposure, and hydrophobic interactions characterize the A adducts, and these are unique for each stereoisomeric adduct. Consequently, mutagenicity and DNA repair properties must be evaluated for each stereoisomeric base adduct to delineate their individual biological effects.

SUPPORTING INFORMATION AVAILABLE

Details of the molecular dynamics protocol and free energy analyses are provided. Table S1 gives glycosidic torsion χ values of the modified adenine, box sizes, and numbers of waters in the MD simulation starting models. Table S2 gives added force field parameters for the modified adenine. Table S3 gives AMBER atom type, connection type, and partial charge assignments for the 4-OHEN-A adducts. Table S4 gives van der Waals interactions between the base pairs. Table S5 gives MM−PBSA free energy components for the 4-OHEN-A modified duplexes. Figure S1 shows starting

structures for the MD simulations. Figure S2 shows rmsd vs time plots for each molecular dynamics simulation. This material is available free of charge via the Internet at http://pubs.acs.org.

REFERENCES

1. Zumoff, B. (1998) Does postmenopausal estrogen administration increase the risk of breast cancer? Contributions of animal, biochemical, and clinical investigative studies to a resolution of the controversy, *Proc. Soc. Exp. Biol. Med. 217*, 30−37.
2. Lupulescu, A. (1995) Estrogen use and cancer incidence: a review, *Cancer Invest. 13*, 287−295.
3. Liehr, J. G. (1990) Genotoxic effects of estrogens, *Mutat. Res. 238*, 269−276.
4. Colditz, G. A., Hankinson, S. E., Hunter, D. J., Willett, W. C., Manson, J. E., Stampfer, M. J., Hennekens, C., Rosner, B., and Speizer, F. E. (1995) The use of estrogens and progestins and the risk of breast cancer in postmenopausal women, *N. Engl. J. Med. 332*, 1589−1593.
5. Hersh, A. L., Stefanick, M. L., and Stafford, R. S. (2004) National use of postmenopausal hormone therapy: annual trends and response to recent evidence, *JAMA 291*, 47−53.
6. Rossouw, J. E., Anderson, G. L., Prentice, R. L., LaCroix, A. Z., Kooperberg, C., Stefanick, M. L., Jackson, R. D., Beresford, S. A., Howard, B. V., Johnson, K. C., Kotchen, J. M., and Ockene, J. (2002) Risks and benefits of estrogen plus progestin in healthy postmenopausal women: principal results From the Women's Health Initiative randomized controlled trial, *JAMA 288*, 321−333.
7. Hays, J., Ockene, J. K., Brunner, R. L., Kotchen, J. M., Manson, J. E., Patterson, R. E., Aragaki, A. K., Shumaker, S. A., Brzyski, R. G., LaCroix, A. Z., Granek, I. A., and Valanis, B. G. (2003) Effects of estrogen plus progestin on health-related quality of life, *N. Engl. J. Med. 348*, 1839−1854.
8. Zhang, F., Chen, Y., Pisha, E., Shen, L., Xiong, Y., van Breemen, R. B., and Bolton, J. L. (1999) The major metabolite of equilin, 4-hydroxyequilin, autoxidizes to an o-quinone which isomerizes to the potent cytotoxin 4-hydroxyequilenin-o-quinone, *Chem. Res. Toxicol. 12*, 204−213.
9. Bolton, J. L., Pisha, E., Zhang, F., and Qiu, S. (1998) Role of quinoids in estrogen carcinogenesis, *Chem. Res. Toxicol. 11*, 1113−1127.
10. Pisha, E., Lui, X., Constantinou, A. I., and Bolton, J. L. (2001) Evidence that a metabolite of equine estrogens, 4-hydroxyequilenin, induces cellular transformation in vitro, *Chem. Res. Toxicol. 14*, 82−90.
11. Chen, Y., Liu, X., Pisha, E., Constantinou, A. I., Hua, Y., Shen, L., van Breemen, R. B., Elguindi, E. C., Blond, S. Y., Zhang, F., and Bolton, J. L. (2000) A metabolite of equine estrogens, 4-hydroxyequilenin, induces DNA damage and apoptosis in breast cancer cell lines, *Chem. Res. Toxicol. 13*, 342−350.
12. Zhang, F., Swanson, S. M., van Breemen, R. B., Liu, X., Yang, Y., Gu, C., and Bolton, J. L. (2001) Equine estrogen metabolite 4-hydroxyequilenin induces DNA damage in the rat mammary tissues: formation of single-strand breaks, apurinic sites, stable adducts, and oxidized bases, *Chem. Res. Toxicol. 14*, 1654−1659.
13. Bolton, J. L., Trush, M. A., Penning, T. M., Dryhurst, G., and Monks, T. J. (2000) Role of quinones in toxicology, *Chem. Res. Toxicol. 13*, 135−160.
14. Liu, X., Yao, J., Pisha, E., Yang, Y., Hua, Y., van Breemen, R. B., and Bolton, J. L. (2002) Oxidative DNA damage induced by equine estrogen metabolites: role of estrogen receptor alpha, *Chem. Res. Toxicol. 15*, 512−519.
15. Bolton, J. L. (2002) Quinoids, quinoid radicals, and phenoxyl radicals formed from estrogens and antiestrogens, *Toxicology 177*, 55−65.
16. Shen, L., Qiu, S., Chen, Y., Zhang, F., van Breemen, R. B., Nikolic, D., and Bolton, J. L. (1998) Alkylation of 2′-deoxynucleosides and DNA by the Premarin metabolite 4-hydroxyequilenin semiquinone radical, *Chem. Res. Toxicol. 11*, 94−101.
17. Luch, A. (2005) Nature and nurture - lessons from chemical carcinogenesis, *Nat. Rev. Cancer 5*, 113−125.
18. Shen, L., Qiu, S. X., van Breemen, R. B., Zhang, F. G., Chen, Y. M., and Bolton, J. L. (1997) Reaction of the Premarin Metabolite 4-Hydroxyequilenin Semiquinone Radical with 2′-Deoxyguanosine: Formation of Unusual Cyclic Adducts, *J. Am. Chem. Soc. 119*, 11126−11127.
19. Embrechts, J., Lemiere, F., Van Dongen, W., and Esmans, E. L. (2001) Equilenin-2′-deoxynucleoside adducts: analysis with nano-liquid chromatography coupled to nano-electrospray tandem mass spectrometry, *J. Mass Spectrom. 36*, 317−328.
20. Embrechts, J., Lemiere, F., Van Dongen, W., Esmans, E. L., Buytaert, P., Van Marck, E., Kockx, M., and Makar, A. (2003) Detection of estrogen DNA-adducts in human breast tumor tissue and healthy tissue by combined nano LC-nano ES tandem mass spectrometry, *J. Am. Soc. Mass Spectrom. 14*, 482−491.
21. Kolbanovskiy, A., Kuzmin, V., Shastry, A., Kolbanovskaya, M., Chen, D., Chang, M., Bolton, J. L., and Geacintov, N. E. (2005) Base selectivity and effects of sequence and DNA secondary structure on the formation of covalent adducts derived from the equine estrogen metabolite 4-hydroxyequilenin, *Chem. Res. Toxicol. 18*, 1737−1747.
22. Ding, S., Shapiro, R., Geacintov, N. E., and Broyde, S. (2003) Conformations of stereoisomeric base adducts to 4-hydroxyequilenin, *Chem. Res. Toxicol. 16*, 695−707.
23. Ding, S., Shapiro, R., Geacintov, N. E., and Broyde, S. (2005) Equilenin-Derived DNA Adducts to Cytosine in DNA Duplexes: Structures and Thermodynamics, *Biochemistry 44*, 14565−14576.
24. Chen, D., Kolbanovskiy, A., Shastry, A., Chang, M., Bolton, J. L., and Geacintov, N. E. (2005) Replication of DNA Sequences with Equine Estrogen Metabolite 4-OHEN-dC Adducts Catalyzed by A- and Y-Family Polymerases in vitro, *Chem. Abstr. 230*, U1853−U1853.
25. Geacintov, N. E., Kolbanovskiy, A., Kuzmin, K., Chang, M. S., and Bolton, J. L. (2003) DNA damage induced by an equine estrogen metabolite (4-OHEN) in solution and the characteristics of site specifically modified oligodeoxynucleotide model systems containing single, stable covalent adducts, *Chem. Res. Toxicol. 16*, 1665−1666.
26. Chen, D. D., Oum, L., Kolbanovskiy, A., Kuzmin, V., Shastry, A., Chang, M. S., Bolton, J. L., and Geacintov, N. (2004) Translesion synthesis and nucleotide excision repair of site specifically modified oligodeoxyribonucleotides containing single lesions derived from the equine estrogen metabolite 4-OHEN, *Chem. Res. Toxicol. 17*, 1782−1782.
27. Suzuki, N., Yasui, M., Santosh Laxmi, Y. R., Ohmori, H., Hanaoka, F., and Shibutani, S. (2004) Translesion Synthesis Past Equine Estrogen-Derived 2′-Deoxycytidine DNA Adducts by Human DNA Polymerases η and κ, *Biochemistry 43*, 11312−11320.
28. Yasui, M., Laxmi, Y. R., Ananthoju, S. R., Suzuki, N., Kim, S. Y., and Shibutani, S. (2006) Translesion Synthesis Past Equine Estrogen-Derived 2′-Deoxyadenosine DNA Adducts by Human DNA Polymerases η and κ, *Biochemistry 45*, 6187−6194.
29. Yasui, M., Matsui, S., Laxmi, Y. R., Suzuki, N., Kim, S. Y., Shibutani, S., and Matsuda, T. (2003) Mutagenic events induced by 4-hydroxyequilin in supF shuttle vector plasmid propagated in human cells, *Carcinogenesis 24*, 911−917.
30. Chen, D. D., Liu, T. M., Ruan, Q., Zou, Y., Kuzmin, V., Kolbanovskiy, A., Chang, M. S., Bolton, J. L., and Geacintov, N. (2003) Nucleotide excision repair of site specific cytidine adducts derived from the equine estrogen metabolite 4-OHEN in DNA by UvrABC proteins from *Escherichia coli*, *Chem. Res. Toxicol. 16*, 1682−1683.
31. Hingerty, B. E., Figueroa, S., Hayden, T. L., and Broyde, S. (1989) Prediction of DNA structure from sequence: a build-up technique, *Biopolymers 28*, 1195−1222.
32. Case, D. A., Darden, T. A., Cheatham, T. E., III, Simmerling, C. L., Wang, J., Duke, R. E., Luo, R., Merz, K. M., Wang, B., Pearlman, D. A., Crowley, M., Brozell, S., Tsui, V., Gohlke, H., Mongan, J., Hornak, V., Cui, G., Beroza, P., Schafmeister, C., and Kollman, P. A. (2004) *AMBER 8*, University of California, San Francisco, CA.
33. Cornell, W. D., Cieplak, P., Bayly, C. I., Gould, I. R., Merz, K. M., Ferguson, D. M., Spellmeyer, D. C., Fox, T., Caldwell, J. W., and Kollman, P. A. (1995) A Second Generation Force Field for the Simulation of Proteins, Nucleic Acids, and Organic Molecules, *J. Am. Chem. Soc. 117*, 5179−5197.
34. Cheatham, T. E., Cieplak, P., and Kollman, P. A. (1999) A modified version of the Cornell et al. force field with improved sugar pucker phases and helical repeat, *J. Biomol. Struct. Dyn. 16*, 845−862.
35. Bayly, C. I., Cieplak, P., Cornell, W. D., and Kollman, P. A. (1993) A Well-Behaved Electrostatic Potential Based Method Using Charge Restraints for Deriving Atomic Charges: the RESP Model, *J. Phys. Chem. 97*, 10269−10280.

36. Zhang, Q., Broyde, S., and Schlick, T. (2004) Deformations of promoter DNA bound to carcinogens help interpret effects on TATA-element structure and activity, *Philos. Trans. R. Soc. London, Ser. A 362*, 1479−1496.
37. Cieplak, P., Cornell, W. D., Bayly, C., and Kollman, P. A. (1995) Application of the Multimolecule and Multiconformational RESP Methodology to Biopolymers - Charge Derivation for DNA, RNA, and Proteins, *J. Comput. Chem. 16*, 1357−1377.
38. Frisch, J. M., Trucks, W. G., Schlegel, B. H., Scuseria, E. G., Robb, A. M., Cheeseman, R. J., Zakrzewski, G. V., Montgomery, A. J., Stratmann, E. R., Burant, C. J., Dappprich, S., Millam, M. J., Daniels, D. A., Kudin, N. K., Strain, C. M., Farkas, O., Tomasi, J., Barone, V., Cossi, M., Cammi, R., Mennucci, B., Pomelli, C., Adamo, C., Clifford, S., Ochterski, J., Petersson, A. G., Ayala, Y. P., Cui, Q., Morokuma, K., Malick, K. D., Rabuck, D. A., Raghavachari, K., Foresman, B. J., Cioslowski, J., Ortiz, V. J., Baboul, G. A., Stefanov, B. B., Liu, G., Liashenko, A., Piskorz, P., Komaromi, I., Comperts, R., Martin, L. R., Fox, J. D., Keith, T., Al-Laham, A. M., Peng, Y. C., Nanayakkara, A., Gonzalez, C., Challacombe, M., Gill, W. M. P., Johnson, B., Chen, W., Wong, W. M., Andres, L. J., Head-Gordon, M., Replogle, S. E., and Pople, A. J. (1998) Gaussian 98, Gaussian, Inc., Pittsburgh, PA.
39. Jorgensen, W. L., Chandrasekhar, J., Madura, J. D., Impey, R. W., and Klein, M. L. (1983) Comparison of Simple Potential Functions for Simulating Liquid Water, *J. Chem. Phys. 79*, 926−935.
40. Darden, T., York, D., and Pedersen, L. (1993) Particle Mesh Ewald - an NLog(N) Method for Ewald Sums in Large Systems, *J. Chem. Phys. 98*, 10089−10092.
41. Essmann, U., Perera, L., Berkowitz, M. L., Darden, T., Lee, H., and Pedersen, L. G. (1995) A Smooth Particle Mesh Ewald Method, *J. Chem. Phys. 103*, 8577−8593.
42. Ryckaert, J. P., Ciccotti, G., and Berendsen, H. J. C. (1977) Numerical-Integration of Cartesian Equations of Motion of a System with Constraints - Molecular-Dynamics of N-Alkanes, *J. Comput. Phys. 23*, 327−341.
43. Harvey, S. C., Tan, R. K. Z., and Cheatham, T. E. (1998) The flying ice cube: Velocity rescaling in molecular dynamics leads to violation of energy equipartition, *J. Comput. Chem. 19*, 726−740.
44. Berendsen, H. J. C., Postma, J. P. M., Vangunsteren, W. F., Dinola, A., and Haak, J. R. (1984) Molecular-Dynamics with Coupling to an External Bath, *J. Chem. Phys. 81*, 3684−3690.
45. Ravishanker, G., Swaminathan, S., Beveridge, D. L., Lavery, R., and Sklenar, H. (1989) Conformational and helicoidal analysis of 30 PS of molecular dynamics on the d(CGCGAATTCGCG) double helix: "curves", dials and windows, *J. Biomol. Struct. Dyn. 6*, 669−699.
46. Ravishanker, G., Wang, W., and Beveridge, D. L. *MD Toolchest*, Wesleyan University, Middletown, CT.
47. Connolly, M. L. (1983) Solvent-accessible surfaces of proteins and nucleic acids, *Science 221*, 709−713.
48. Srinivasan, J., Cheatham, T. E., Cieplak, P., Kollman, P. A., and Case, D. A. (1998) Continuum Solvent Studies of the Stability of DNA, RNA, and Phosphoramidate-DNA Helices, *J. Am. Chem. Soc. 120*, 9401−9409.
49. Kollman, P. A., Massova, I., Reyes, C., Kuhn, B., Huo, S., Chong, L., Lee, M., Lee, T., Duan, Y., Wang, W., Donini, O., Cieplak, P., Srinivasan, J., Case, D. A., and Cheatham, T. E., III (2000) Calculating Structures and Free Energies of Complex Molecules: Combining Molecular Mechanics and Continuum Models, *Acc. Chem. Res.* 33, 889−897.
50. Wang, W., and Kollman, P. A. (2000) Free energy calculations on dimer stability of the HIV protease using molecular dynamics and a continuum solvent model, *J. Mol. Biol. 303*, 567−582.
51. Reyes, C. M., and Kollman, P. A. (2000) Structure and thermodynamics of RNA-protein binding: using molecular dynamics and free energy analyses to calculate the free energies of binding and conformational change, *J. Mol. Biol. 297*, 1145−1158.
52. Lee, M. R., Duan, Y., and Kollman, P. A. (2000) Use of MM-PB/SA in estimating the free energies of proteins: application to native, intermediates, and unfolded villin headpiece, *Proteins 39*, 309−316.
53. Wang, J., Morin, P., Wang, W., and Kollman, P. A. (2001) Use of MM-PBSA in Reproducing the Binding Free Energies to HIV-1 RT of TIBO Derivatives and Predicting the Binding Mode to HIV-1 RT of Efavirenz by Docking and MM-PBSA, *J. Am. Chem. Soc. 123*, 5221−5230.
54. Huo, S., Massova, I., and Kollman, P. A. (2002) Computational alanine scanning of the 1:1 human growth hormone-receptor complex, *J. Comput. Chem. 23*, 15−27.
55. Honig, B., and Nicholls, A. (1995) Classical electrostatics in biology and chemistry, *Science 268*, 1144−1149.
56. Nicholls, A., Sharp, K. A., and Honig, B. (1990) *Delphi*, Department of Biochemistry and Molecular Biophysics, Columbia University, New York.
57. Sitkoff, D., Sharp, K. A., and Honig, B. (1994) Accurate Calculation of Hydration Free-Energies Using Macroscopic Solvent Models, *J. Phys. Chem. 98*, 1978−1988.
58. Alberts, B., Bray, D., Lewis, J., Raff, M., Roberts, K., and Watson, J. D. (1994) *Molecular Biology of the Cell*, 3rd eD, Garland Publishing, Inc., New York.
59. Gilson, M. K., and Honig, B. H. (1987) Calculation of Electrostatic Potentials in an Enzyme Active-Site, *Nature 330*, 84−86.
60. Sanner, M. F., Olson, A. J., and Spehner, J. C. (1996) Reduced surface: an efficient way to compute molecular surfaces, *Biopolymers 38*, 305−320.

BI061652O